2010-02

Aharonov-Bohm interference in neutral excitons: effects of built-in electric fields

Physical Review Letters, College Park : American Physical Society

Remover selecionados - APS, 2010

http://www.producao.usp.br/handle/BDPI/49641

Aharonov-Bohm Interference in Neutral Excitons: Effects of Built-In Electric Fields

M. D. Teodoro,[1,2] V. L. Campo, Jr.,[1] V. Lopez-Richard,[1,*] E. Marega, Jr.,[3,2] G. E. Marques,[1] Y. Galvão Gobato,[1] F. Iikawa,[4] M. J. S. P. Brasil,[4] Z. Y. AbuWaar,[5,2] V. G. Dorogan,[2] Yu. I. Mazur,[2] M. Benamara,[2] and G. J. Salamo[2]

[1]*Departamento de Física, Universidade Federal de São Carlos, 13565-905, São Carlos, São Paulo, Brazil*
[2]*Arkansas Institute for Nanoscale Materials Science and Engineering, University of Arkansas, Fayetteville, Arkansas 72701, USA*
[3]*Instituto de Física de São Carlos, Universidade de São Paulo, 13.566-590, São Carlos, São Paulo, Brazil*
[4]*Instituto de Física "Gleb Wataghin", Universidade Estadual de Campinas, 13083-970, Campinas, São Paulo, Brazil*
[5]*Department of Physics, University of Jordan, Amman 11942, Jordan*

(Received 24 August 2009; published 22 February 2010)

We report a comprehensive discussion of quantum interference effects due to the finite structure of neutral excitons in quantum rings and their first experimental corroboration observed in the optical recombinations. The signatures of built-in electric fields and temperature on quantum interference are demonstrated by theoretical models that describe the modulation of the interference pattern and confirmed by complementary experimental procedures.

DOI: 10.1103/PhysRevLett.104.086401 PACS numbers: 71.35.Ji, 73.21.La, 78.20.Ls

The nanoscale ring structures, or quantum rings (QRs), have attracted the interest of the scientific community due to their unique rotational symmetry and the possibility to verify quantum mechanical phenomena [1–4]. Among these, the study of Aharonov-Bohm (AB)-like effects have been of special interest [5–7]. In fact, these efforts have gone beyond the original discussion of the AB interpretation on the nature of electromagnetic potentials and their role in quantum mechanics [8]. In most cases the study of coherent interference in the transport properties of nanoscopic QRs, as in Ref. [8], have encountered serious scale limitations, encouraging the search for optical measurements associated to AB effects.

Although real QRs do not meet the original conditions for the AB configuration, since the carriers move within regions with finite values of magnetic field, we can still consider an observed effect as of AB type if it can be explained assuming that the magnetic field is ideally concentrated in the middle of the QRs, coming, essentially, from a vector potential-modulated interference.

In this work, we demonstrated experimentally for the first time the AB interference in excitonic states as proposed theoretically in Refs. [9–12]. We focus on the excitonic oscillator strength (OS) during photoluminescence (PL) whose oscillatory behavior reflects directly the changes in the exciton wave function as the magnetic flux increases. Instead focusing on type-II quantum dots (QDs), [7] here we report the AB effect in type-I systems where both electron and hole move together in the ring, making the correlation between them crucial to the oscillatory behavior found in the PL integrated intensity.

The samples were grown by molecular beam epitaxy. A comprehensive and detailed description of the formation of these sets of self-assembled QRs can be found in Ref. [13]. Atomic force microscopy (AFM) was used to investigate the surface morphology of the grown nanostructures as depicted in Fig. 1(a), where an uncapped sample of InAs QRs is shown with a typical density of about 2.4×10^{10} cm^{-2}. The sample was capped with a 50 nm GaAs layer and subsequent morphological and structural analysis was carried out using transmission electron microscopy (TEM) [Figs. 1(b) and 1(c)].

We performed magneto-PL experiments in self-assembled InAs/GaAs QRs structures. They present a broad optical emission band (~60 meV) measured at 2 K, as shown in Fig. 1(d), and a weak shoulder (~40 meV) in the low energy range, labeled QR2 and

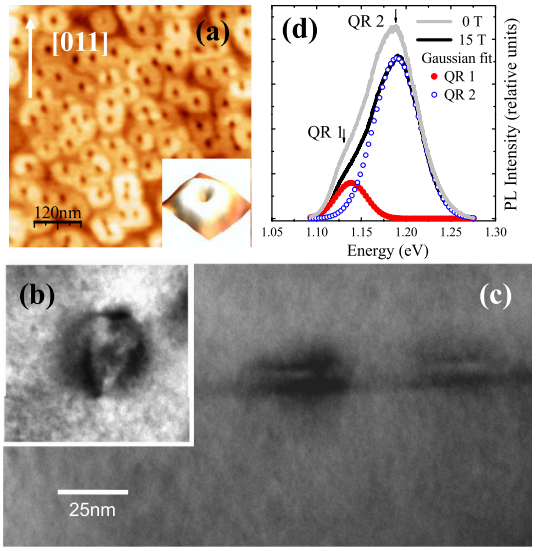

FIG. 1 (color online). (a) AFM image of an uncapped InAs QR sample (3D ring profile in inset). (b) plan-view bright-field TEM image of a ring taken close to the [001] zone axis with [220] reflecting planes. (c) High-resolution TEM image on cross-section samples providing ring thickness and confirming that they lie on {001} planes. (d) PL spectra of the InAs QRs for $B = 0$ T and $B = 15$ T at 2 K. For both spectra there are two radiative channels, QR 1 and QR 2.

QR1, respectively. We used Gaussian functions to fit two emission bands attributed to the bimodal QR distribution dominated, in this case, by high energy QRs. Under an external magnetic field applied along the growth direction, we observed the expected blue shift of both emission bands.

The energy of the PL peak position as a function of the magnetic field presented in Figs. 2(a) and 2(b) also shows small oscillations that could be related to an AB-like effect. Nonetheless, the amplitude of those oscillations (~0.5 meV) is relatively small as compared to the linewidth of the PL bands (~60 meV), making the uncertainty involved on this result relatively large, specially for the QR1 band which appears as a shoulder of the dominant QR2 band. The uncertainty concerning the results of the integrated intensity of the PL bands [Figs. 2(c) and 2(d)] is, however, relatively smaller.

Two features emerge: (i) the oscillations for QR1 and QR2 have different periods and (ii) their maxima and minima occur in opposite sequence. The first implies different average radius for QR1 and QR2 (11.6 and 22.5 nm, respectively) since each oscillation corresponds to a magnetic flux increase of one quantum of flux, $\Phi_0 = hc/e$. The second feature, the opposite sequence of maxima and minima for QR1 and QR2, is the central question discussed in this Letter. According to the simplified model of one interacting e-h pair in a ring of zero-width, [9,10] at $T = 0$ K and in the absence of electric field we should have an oscillatory pattern like that for QR1 in Fig. 2(c), whereas a pattern like that for QR2 [Fig. 2(d)] could arise at higher temperatures or in the presence of an in-plane electric field

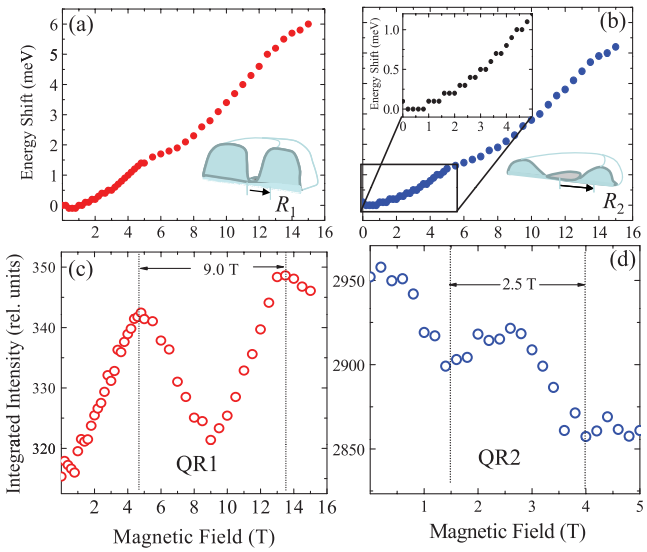

FIG. 2 (color online). PL energy peak position vs magnetic field from emission band (a) QR1, with visible AB-oscillations and (b) QR2, with unclear AB-oscillations. (c) and (d) show the integrated PL intensity of QR1 and QR2 vs magnetic field, respectively, both displaying clear AB-oscillations. The higher transition energy and the larger average radius of QR2, suggests it may present smaller ring width and height than QR1.

[12]. We will present convincing arguments to support the existence of a built-in electric field originated by piezoelectricity.

To formulate a consistent picture of correlation between AB interference and e-h interaction, we consider a simplified model where electron and hole move in a zero-width ring of radius R threaded by a magnetic flux $\Phi = \pi R^2 B$ and interact by means of a contact potential [9,10,12]. Within the symmetric gauge [8], the model Hamiltonian is given by

$$\hat{H}_0 = \frac{(\hat{P}_e + \frac{e\Phi}{2\pi Rc})^2}{2m_e} + \frac{(\hat{P}_h - \frac{e\Phi}{2\pi Rc})^2}{2m_h} - V\delta(\theta_e - \theta_h), \quad (1)$$

where $\theta_{e(h)}$ is the angular position of electron (hole) and $\hat{P}_{e(h)} = \frac{\hbar}{iR}\partial/\partial\theta_{e(h)}$. The interaction strength V has been chosen so that the corresponding exciton binding energy be equal to 4.35 meV [14].

This Hamiltonian becomes separable if we change to the center-of-mass and relative position coordinates, $\Lambda = (m_e\theta_e + m_h\theta_h)/M$, $\theta = \theta_e - \theta_h$, respectively, where $M = m_e + m_h$. The exciton eigenfunction will be

$$\Psi(\Lambda, \theta) = \frac{e^{iJ\Lambda}}{\sqrt{2\pi}} e^{-i(\Phi/\Phi_0)\theta}\chi(\theta), \quad (2)$$

where the function χ satisfies Bloch's theorem and the twisted boundary condition [9]

$$\chi(\pi) = e^{i2\pi p}\chi(-\pi), \quad (3)$$

where p can be restricted to the reduced Brillouin zone, $p \in (-1/2, 1/2]$. Note that $|\chi(\theta)|^2$ represents the probability density of finding the electron and hole angular positions differing by θ. The periodicity of $\Psi(\Lambda, \theta)$ in θ_e and θ_h determines that J and $\gamma J + 2(\Phi/\Phi_0 - p)$ must be integer numbers with same parity [9]. Figure 3(a) illustrates the dependence of the exciton spectrum on magnetic flux.

The behavior of the OS is unambiguously related to the relative motion of the electron and the hole given by the function χ in Eq. (2). The OS of the ground state, $J = 0$, is given by

$$I_0 = \left| \int_0^{2\pi} \Psi(\Lambda, 0) d\Lambda \right|^2 = \frac{|\chi(0)|^2}{2\pi}, \quad (4)$$

being a periodic function on the magnetic flux, as represented in Fig. 3(b) ($T = 0$ K). In the calculations, the InAs band parameters used were: the in-plane masses $m_h = (\gamma_1 + \gamma_2)^{-1}$ and $m_e = 0.026$, where $\gamma_1 = 20.4$, and $\gamma_2 = 8.3$ [14]. Note that we used the heavy-hole (HH)-mass in the (100) plane, assuming that the light-hole (LH) exciton, with mass $m_h = (\gamma_1 - \gamma_2)^{-1}$, occupies a higher energy position due to strain effects. In order to understand the oscillations, as shown in Fig. 3(b), in terms of AB-like interference, we have displayed the function $|\chi|^2$ for zero flux and for $\Phi/\Phi_0 = 1/2$, in Fig. 3(c). For $\Phi/\Phi_0 = 1/2$, the exciton wave-function χ satisfies antiperiodic bound-

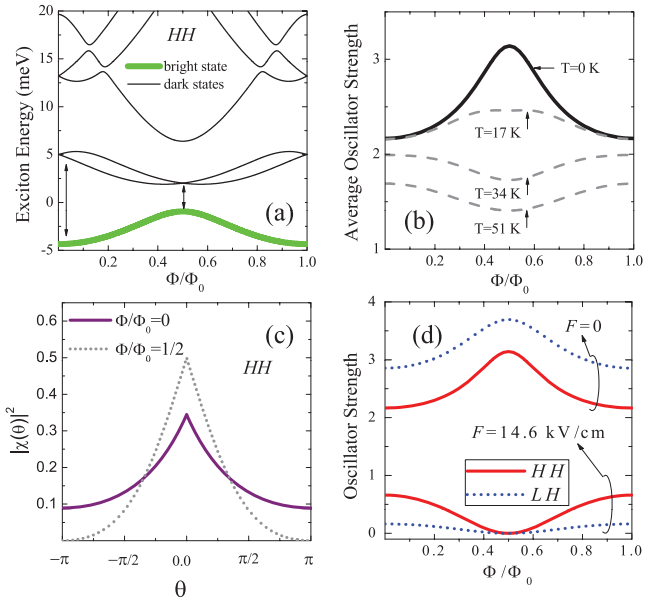

FIG. 3 (color online). (a) Magnetic flux dependence of the (HH)-exciton spectrum (binding energy $E_b = 4.35$ meV). (b) OS as a function of magnetic flux for a (HH) exciton at various temperatures. (c) Probability density of finding the electron and (HH) angular positions differing by θ. (d) Ground-state OS for the (HH) exciton (solid curve) and the (LH) exciton (dashed curve) as a function of the magnetic flux at two values of an in-plane electric field.

ary condition [Eq. (3)] yielding the cancellation of the probability density at $\theta = \pm\pi$ and stronger wave-function confinement near $\theta = 0$. Without e-h interaction the correlation between the electron and hole disappears and the oscillations of the OS vanish. The Coulomb interaction, even with short range character, leads to a rather peculiar AB-interference detected optically as oscillations of the PL emission intensity [11].

In order to take into account the temperature, we generalize Eq. (4) to include all excitonic states, $I(T) = \sum_n I_n e^{-E_n/k_BT}/\sum_n e^{-E_n/k_BT}$, where I_n is the OS for the nth state, $I_n = |\int_0^{2\pi} \Psi_n(\Lambda, 0) d\Lambda|^2$. As the temperature rises, the probability of occupation of the exciton excited levels increases [15]. In Fig. 3(a) the exciton energy levels are displayed for (HH) excitons where the first excited levels correspond to dark excitons. By increasing the flux, starting from $\Phi/\Phi_0 = 0$ up to $\Phi/\Phi_0 = 1/2$, the dark exciton levels approach the bright one. At finite temperature, the net occupation of the ground state decreases, reducing the thermalized OS. At relatively high temperatures, this effect transforms the maximum of the OS at $\Phi/\Phi_0 = 1/2$ into a minimum for the (HH) exciton, as displayed in Fig. 3(b).

The inversion of the maximum of the OS for the exciton ground state can also be due to the existence of an in-plane electric field which can be caused by uniaxial strains and the subsequent piezoelectricity, that can be relatively strong in InGaAs self-assembled 0D structures [16,17]. The in-plane electric field F along the x axis can be introduced into the model Hamiltonian as $\hat{H} = \hat{H}_0 + eFR(\cos(\theta_e) - \cos(\theta_h))$. In order to solve this problem, we adopted a basis set of eigenfunctions of $\hat{H}_0$ [Eqs. (1) and (2)] to expand the new solutions. Note that the electric field only couples states whose center-of-mass angular momenta [J in Eq. (2)] differ by one. We can expect that the OS will decrease with increasing electric field, since the electron and the hole are pushed apart. Figure 3(d) illustrates the inversion of the maximum in the curves of OS against magnetic flux at $T = 0$ K for both (HH) and (LH) excitons as a result of increasing the in-plane electric field. Above a critical value of the electric field, the oscillation pattern becomes inverted [12]. The stronger the electric field, the higher is the projection of the ground state over states with odd angular function, χ. This is particularly important at $\Phi/\Phi_0 = 1/2$ beyond the critical field, when the ground state is a pure odd function with null OS [12]. Certainly, for a QR with finite width, this extreme reduction is not expected.

The effects of built-in electric fields in the rings mentioned above has already been described in previous works [17]. During the QR growth, anisotropic strain fields are formed in the (001) plane leading to an elongation of the ring in the $[1\bar{1}0]$ direction [13] and a built-in electric field due to the piezoelectric effect. Additional optical experiments show the evidence of the presence of built-in electric fields in QR2 and negligible field values in QR1, which is consistent with the models discussed above. Figure 4 shows the PL spectra vs excitation intensity. Increasing the excitation intensity, we observed additional emission bands in high energy side region, which are attributed to the filling of the excited states of QR2 (dominant band). As

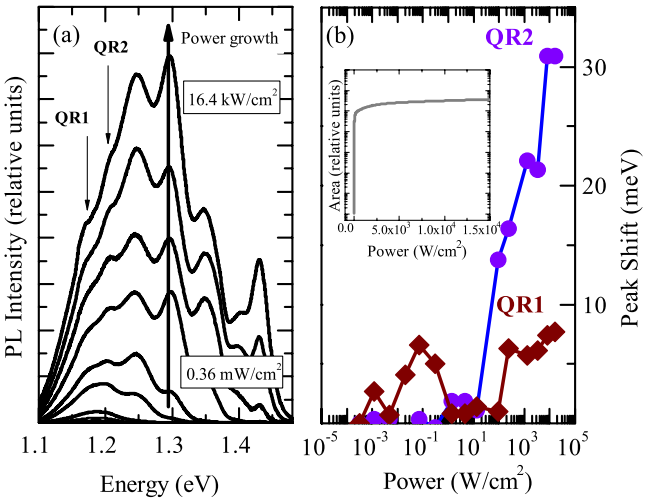

FIG. 4 (color online). (a) Series of the PL emission for increasing excitation powers from 0.36 mW/cm^2 to 16.4 kW/cm^2. (b) Position of emission peaks vs excitation power. The inset shows the log-log relative area (ratio of peak 2 area to peak 1 area), which displays two distinct lines, at low and high excitation power, the fingerprint of excitons in semiconductors nanostructures.

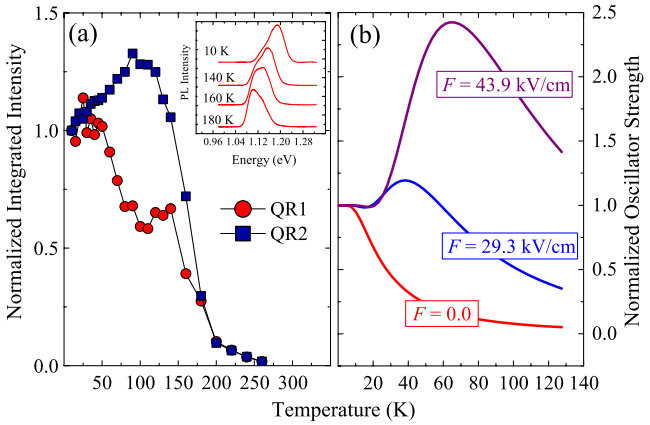

FIG. 5 (color online). (a) PL integrated intensity normalized to the value at $T = 10$ K, for the emission bands QR1 and QR2, respectively. (b) Calculated OS (normalized to the value at $T = 0$) for three values of the in-plane electric field F. The increase of PL intensity at low temperatures can be understood as an electric field effect. Inset: PL spectra at low temperature are dominated by the emission band QR2, whereas above 160 K, they become dominated by QR1, which is attributed to the transference of carriers between QRs, via wetting layer, favoring the lower energy states, as also observed in QD systems.

the carrier population in the QRs increases at higher laser intensities, the built-in electric field should be screened. In Fig. 4(b) we plotted the energy shift of the QR1 and QR2 versus excitation intensity. We observed a blueshift of the emission band QR2 at the high excitation regime, suggesting the screening of the built-in electric field. The blueshift is not observed in the emission band QR1 whose peak energy remains practically constant, confirming thus that the built-in electric field in those QRs is negligible. The unclear point, however, is why the built-in electric field related to the band QR1 is negligible, since the effect of the elongation should be applied for all rings. A possible reason is that the ring width corresponding to QR1 is larger than that for QR2, as mentioned above and the strain field relief for the former may be stronger than for the latter, resulting in a much lower piezoelectric field.

We also investigated the temperature dependence of the excitonic emissions in QR. In Fig. 5(a), the integrated intensity for each emission band vs temperature is plotted. The decrease of the PL intensity is expected, due to the occupation of dark excitonic states. However, we observed an increase of the intensity for QR2 at $T < 100$ K. This is another signature of the presence of an in-plane electric field in these QRs as corroborated theoretically by the results shown in Fig. 5(b). With electric field, the OS can increase by the activation of more efficient channels for optical recombination at excited states with e-h angular separation smaller than in the ground state.

These experimental results confirm that the inversion in the sequence of minima and maxima for the band QR2, in Fig. 2(d), cannot be attributed to effects induced by temperature, since only for $T > 150$ K an effective reduction of the ground-state occupation takes place [far above the temperature of 2 K where the oscillations in Fig. 2(d) were detected]. Therefore we attribute the sequence of minima and maxima observed in the intensity oscillations of QR2 to the effect associated to AB interference combined with the in-plane electric field.

In summary, we have introduced a theoretical picture for an AB effect in nanoscopic QRs and its modulation by temperature and built-in electric fields. These effects were experimentally observed and characterized by using optical methods. The AB oscillations can be traced by patterns of the PL intensity under increasing magnetic field and the built-in piezoelectric fields may have an important role in strained QR systems by changing the sequence of maxima and minima of these oscillations. The Coulomb interaction is crucial for the observations reported here. Without it, the correlation between electrons and holes vanishes and the oscillations disappear.

The authors are grateful to the Brazilian Agencies FAPESP, CNPq, and CAPES for financial support and to the National Science Foundation of the U. S. through Grant DMR-0520550.

*vlopez@df.ufscar.br

[1] J. M. García *et al.*, Appl. Phys. Lett. **71**, 2014 (1997).
[2] A. Lorke *et al.*, Phys. Rev. Lett. **84**, 2223 (2000).
[3] F. M. Alves, C. Trallero-Giner, V. Lopez-Richard, and G. E. Marques, Phys. Rev. B **77**, 035434 (2008).
[4] N. A. J. M. Kleemans *et al.*, Phys. Rev. B **80**, 155318 (2009).
[5] M. Grochol, F. Grosse, and R. Zimmermann, Phys. Rev. B **74**, 115416 (2006).
[6] P. A. Orellana and M. Pacheco, Phys. Rev. B **71**, 235330 (2005).
[7] I. R. Sellers *et al.*, Phys. Rev. Lett. **100**, 136405 (2008).
[8] Y. Aharonov and D. Bohm, Phys. Rev. **115**, 485 (1959).
[9] A. V. Chaplik, Pis'ma Zh. Eksp. Teor. Fiz. **62**, 885 (1995) [JETP Lett. **62**, 900 (1995)].
[10] R. A. Römer and M. E. Raikh, Phys. Rev. B **62**, 7045 (2000); Phys. Status Solidi B **221**, 535 (2000).
[11] T. Chakraborty and P. Pietiläinen, Phys. Rev. B **50**, 8460 (1994).
[12] Andrea M. Fischer, V. L. Campo, Jr., M. E. Portnoi, and R. A. Röomer, Phys. Rev. Lett. **102**, 096405 (2009).
[13] M. Hanke *et al.*, Appl. Phys. Lett. **91**, 043103 (2007).
[14] *Landölt-Börnstein Comprehensive Index*, edited by O. Madelung and W. Martienssen (Springer, Berlin, 1996).
[15] C. H. Lin *et al.*, Appl. Phys. Lett. **94**, 183101 (2009).
[16] A. Schliwa, M. Winkelnkemper, and D. Bimberg, Phys. Rev. B **76**, 205324 (2007).
[17] J. A. Barker, R. J. Warburton, and E. P. O'Reilly, Phys. Rev. B **69**, 035327 (2004).